UC-94c
LBL-18575
Preprint c.1

Lawrence Berkeley Laboratory

UNIVERSITY OF CALIFORNIA

RECEIVED
LAWRENCE
BERKELEY LABORATORY
DEC 19 1984
LIBRARY AND
DOCUMENTS SECTION

Materials & Molecular Research Division

Submitted to the Journal of the Electrochemical Society

INTERFEROMETRIC OBSERVATION OF TURBULENT MASS TRANSFER IN CHANNEL FLOW

F.R. McLarnon, R.H. Muller, and C.W. Tobias

October 1984

For Reference

Not to be taken from this room

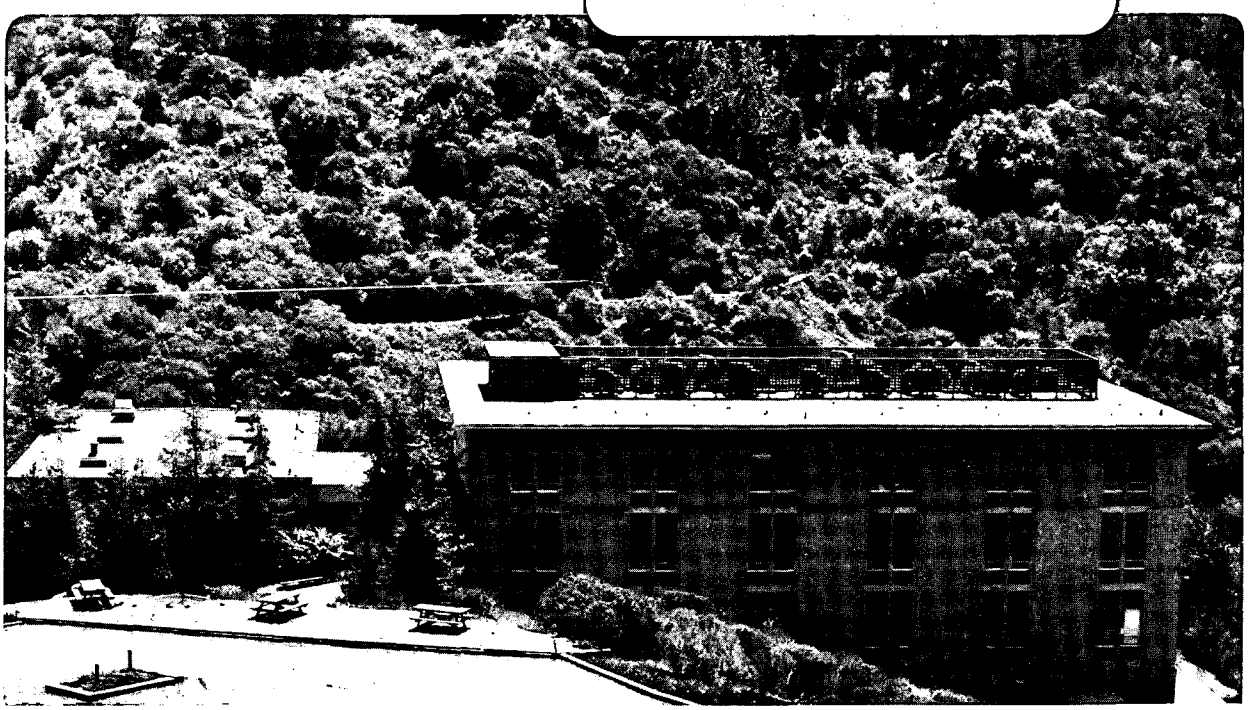

LBL-18575 c.1

Prepared for the U.S. Department of Energy under Contract DE-AC03-76SF00098

DISCLAIMER

This document was prepared as an account of work sponsored by the United States Government. While this document is believed to contain correct information, neither the United States Government nor any agency thereof, nor the Regents of the University of California, nor any of their employees, makes any warranty, express or implied, or assumes any legal responsibility for the accuracy, completeness, or usefulness of any information, apparatus, product, or process disclosed, or represents that its use would not infringe privately owned rights. Reference herein to any specific commercial product, process, or service by its trade name, trademark, manufacturer, or otherwise, does not necessarily constitute or imply its endorsement, recommendation, or favoring by the United States Government or any agency thereof, or the Regents of the University of California. The views and opinions of authors expressed herein do not necessarily state or reflect those of the United States Government or any agency thereof or the Regents of the University of California.

LBL-18575

INTERFEROMETRIC OBSERVATION OF TURBULENT MASS TRANSFER IN CHANNEL FLOW*

F.R. McLarnon

Applied Science Division, Lawrence Berkeley Laboratory,
University of California
Berkeley, California 94720

R.H. Muller and C.W. Tobias

Materials and Molecular Research Division, Lawrence Berkeley Laboratory,
and Department of Chemical Engineering, University of California,
Berkeley, California 94720

October 1984

* This work was supported by the Director, Office of Energy Research, Office of Basic Energy Sciences, Materials Sciences Division of the U.S. Department of Energy under Contract No. DE-AC03-76SF00098.

ABSTRACT

A traveling, dual-beam laser interferometer has been used to investigate mass-transfer boundary layers on planar electrodes in turbulent channel flow. The effect of secondary flows induced near the electrode/electrolyte interface by small flow obstacles in laminar bulk flow is compared to the effect of turbulent bulk flow produced by high electrolyte flow rates in an obstacle-free flow channel. It is shown that mass-transfer enhancement can be attained more efficiently by the use of small flow obstacles than by the use of high flow velocities.

Key words: electrodeposition; mass transfer; convection; interferometry; cathode.

INTERFEROMETRIC OBSERVATION OF TURBULENT MASS TRANSFER IN CHANNEL FLOW

F.R. McLarnon

Applied Science Division, Lawrence Berkeley Laboratory,
Berkeley, California 94720

R.H. Muller and C.W. Tobias

Materials and Molecular Research Division, Lawrence Berkeley Laboratory,
and Department of Chemical Engineering, University of California,
Berkeley, California 94720

ABSTRACT

A traveling, dual-beam laser interferometer has been used to investigate mass-transfer boundary layers on planar electrodes in turbulent channel flow. The effect of secondary flows induced near the electrode/electrolyte interface by small flow obstacles in laminar bulk flow is compared to the effect of turbulent bulk flow produced by high electrolyte flow rates in an obstacle-free flow channel. It is shown that mass-transfer enhancement can be attained more efficiently by the use of small flow obstacles than by the use of high flow velocities.

Key words: electrodeposition; mass transfer; convection; interferometry; cathode.

INTRODUCTION

Turbulent fluid flow can often be successfully employed to increase interfacial transport rates in a variety of industrial unit operations. Many electrochemical processes, such as electrowinning, electrochemical synthesis, and electrodialysis, tend to be rate-limited by slow mass transfer. The application of turbulent in place of laminar electrolyte flow in these processes permits higher operating current densities and thereby improves the space-time yield of the electrochemical system. The most direct method to induce turbulent flow in an electrochemical cell is to raise the electrolyte velocity(1), but this technique may result in an unacceptable increase in electrolyte pumping power(2). Other viable methods include insertion of flow obstacles into the electrolyte flow stream(3), moving nets across the electrode surface(4), applying magnetic fields(5) or ultrasonic waves(6), and use of suspended particles(7).

The limiting-current technique(8) is a powerful tool that has been used by many investigators(9) to characterize the local distribution of mass transfer rates at electrode surfaces under conditions of turbulent flow. Of particular relevance to the present study are applications of the limiting-current technique(3,10-18) to evaluate the enhancement of mass-transfer rates by placing flow obstacles in the electrolyte flow stream. These investigations have provided valuable data to guide the optimal selection of fluid flow rates, cell geometry, and promoter shape, size, and spacing.

The purpose of the present work is to employ interferometry(19,20) to characterize mass-transfer enhancement by turbulent flow, thereby

providing data complementary to those obtained by the limiting-current technique. In this method, local variations in the phase of transmitted light are measured, and the corresponding variations in refractive index (linearly related to concentration under the conditions of this study) are subsequently derived. The technique provides direct, continuous visualization of the local concentration boundary layer at any level of current density on continuous (unsectioned) electrodes. The interferometric method has been previously applied to study electrochemical mass transfer under conditions of pure diffusion(21-24), natural convection(25-29), forced convection(30-32), combined forced and natural convection(33), and turbulent flow(32,34).

EXPERIMENTAL

Flow channel. - Mass-transfer experiments were carried out in a 3-m long rectangular-duct flow channel(35-37), the heart of which is depicted in Fig. 1. Gravity feed from a storage tank provides a steady flow of electrolyte. The duct is w = 1.00 cm wide and h = 2.54 cm high. The L = 100 cm long electrodes fully occupy the space between the two parallel, optically-flat glass sidewalls downstream of a 200-cm long (140 hydraulic diameters) entry region. All experiments were performed with the cathode facing down and the anode facing up. This configuration will produce less-dense electrolyte regions above more-dense regions, eliminating the possibility of electrolyte flow induced by natural convection. The primary current density distribution in this cell was calculated(31) to be nearly uniform; local current densities deviate from the average current density by no more than 1% for 97% of the electrode

surface. The deviations from uniform primary current density occur only within a few centimeters of the coplanar junctions between conductor and insulator, i.e. at the leading and trailing edges of the electrode. When current is passing, the electric field effect (and the associated small nonuniformity of the primary current density distribution) is moderated by the presence of charge-transfer and mass-transfer overpotentials. The resulting tertiary current distribution is even more uniform than the primary distribution. Near the limiting current density, the current distribution reflects local variations in mass-transfer boundary layer thickness.

Flow Obstacles. - Experiments were performed with five different obstacles placed in the flow channel. Figure 2 schematically illustrates the shapes and sizes of the obstacles relative to the local mass-transfer boundary layer thickness. The largest obstacle is a 12.7-mm diameter, 10.0-mm long glass circular cylinder sandwiched between the two glass sidewalls, midway between the two electrodes. This object occupies 50% of the channel cross-section, and it can create turbulence by increasing the local electrolyte flow velocity. The other four obstacles shown in Fig. 2 are a rectangular parallelepiped, a triangular parallelepiped, and two semi-circular cylinders. All four of these obstacles, extending across the entire 10.0-mm channel width, were machined from acrylic, and were glued to the cathode surface. The three larger obstacles extend 0.76 mm from the cathode surface and occupy 3% of the channel cross-section. The smallest obstacle extends 0.28 mm from the cathode surface and occupies only 1% of the channel cross-section. The dashed curves in

Fig. 2 indicate the edge of the 99% mass-transfer boundary layer* predicted(38,2,9) for laminar flow conditions (Re = 500 and Re = 1500). Figure 2 shows that the dimensions of the smaller obstacles are comparable to those of the mass-transfer boundary layers expected under laminar flow conditions.

Electrolyte and electrode preparation. - The 99.999%-pure copper electrodes were designed with two goals in mind: (i) the horizontal electrode surfaces should be flat and smooth, and (ii) the test beam should traverse the cell parallel to the surface. These requirements were met by first polishing a vertical side of each electrode flat and optically smooth. Then, a right-angle polishing jig was used to prepare the electrode working surfaces perpendicular to the reflecting sides. The cell would then be aligned so that the test beam was parallel (to within 0.1°) to the electrode working surface by reflecting the beam from the side under exactly normal incidence (the reflected beam retraced its path back to its source). The working surface profile was flat to with 1 μm over 80% of its width. However, the edges were very slightly rounded (to about 10 μm) below the level of the center of the surface.**

The aqueous $CuSO_4$ electrolyte was prepared by dissolving reagent-grade $CuSO_4 \cdot 5H_2O$ crystals into twice-distilled water in a 25 gal polyethylene container. The dependence of electrolyte refractive index

* The distance from the electrode surface where the local concentration reaches the sum of the surface concentration plus 99% of the total concentration difference (bulk less surface).

** This small deviation from planarity has been shown(39) to result in reflection of the test beam from the rounded electrode edge, which can cause anomalous curvature of the interference fringes in the immediate vicinity of the electrode surface.

on $CuSO_4$ concentration was determined with an Abbe′ critical angle refractometer. Sample concentrations were determined by gravimetric analysis. Least-squares analysis provided a linear correlation for the refractive index at λ =632.8 nm (He-Ne laser), $0 \leq C \leq 0.1M$ $CuSO_4$, 20°C. All electrolysis experiments employed 0.1M $CuSO_4$ electrolyte and were conducted at 20°C in 0.1M $CuSO_4$.

Interferometer. - A cross section of the duct and dual-emission laser interferometer is shown in Fig. 3. A He-Ne laser was modified to emit light from each end of the laser cavity, and the interferometer was mounted on the carriage of a lathe bed to permit travel of the instrument along the length of the electrodes(35-37). The plane of focus (optically conjugate to the film plane of the camera) was located at the inside of the glass sidewall farthest from the camera, x = 0 (Fig. 1). This is the recommended plane of focus for the observation of cathodic boundary layers in which the refractive index decreases toward the electrode surface(40).

Electrochemical experiments. - Steady-state, constant-current electrodeposition of Cu onto a downward-facing cathode was studied at Re = 500, 1500, 5,000 and 10,000 (v_{avg} = 3.5, 10.5, 35 and 70 cm/sec, respectively). Average current densities ranged from 2.0 to 25.0 mA/cm^2. Local limiting current densities under laminar flow conditions at the trailing edge of the cathode surface ranged from 3.8 mA/cm^2 at Re = 500 to 5.5 mA/cm^2 at Re = 1500. Average limiting current densities under turbulent flow conditions ranged from 34 mA/cm^2 at Re = 5,000 to 56 mA/cm^2 at Re = 1500. Average applied current densities are listed in

Table 1. Note that limiting current densities are not approached, except near the trailing edge of the cathode for the single experiment at Re = 500 and i_{avg} = 5.0 mA/cm^2, which was performed for qualitative comparison purposes only.

The five obstacles were placed in the flow channel for some of the laminar flow experiments (Re = 500 and 1500); no flow obstacles were employed for the turbulent-flow experiments (Re = 5,000 and 10,000).

Table 1

Experimental Matrix

v_{avg}(cm/sec)	Re	i_{avg} (mA/cm^2)	Flow Obstacles Present
3.5	500	2.0	yes
3.5	500	5.0	no
10.5	1500	2.5	yes
10.5	1500	5.0	no
35	5,000	15.0	no
35	5,000	25.0	no
70	10,000	25.0	no

RESULTS AND DISCUSSION

The effect of electrolyte flow velocity on the steady-state mass-transfer boundary layer, formed by constant-current electrodeposition of Cu from 0.1M $CuSO_4$ without obstacles in the flow channel, is illustrated in Fig. 4. The curvature of the interference fringes seen near the electrode surface indicates reduced $CuSO_4$ concentration in the mass-transfer boundary layer. In this region, the electrolyte refractive index is lower than that in the bulk electrolyte, where the interference fringes are straight and perpendicular to the plane of the electrode surface. To a first approximation, the shape of an interference fringe represents the $CuSO_4$ concentration profile, with a displacement of one fringe spacing corresponding to a concentration change of 0.0022M $CuSO_4$. Inspection of Fig. 4 leads to the following observations:

1. Increasing the electrolyte flow velocity from Re = 500 to Re = 10,000 reduces the mass-transfer boundary layer thickness from (approximately) 1 mm to 0.1 mm.

2. The interfacial concentration gradient appears to be similar in all four experiments, even though the current density varies by a factor of five.

3. The apparent location of the electrode/electrolyte interface shows considerable deviation from its actual location, marked by the "0" ordinate designation, observed in the absence of refractive-index gradients. In the absence of mass-transfer boundary layers, the interference fringes are arranged to be straight and

perpendicular to the plane of the electrode surface. There is, however, a very slight curvature of the fringes within 0.02 mm of the electrode surface, caused by reflection from the very slightly rounded edge of the electrode surface(39).

4. The decrease of electrolyte concentration at the interface (relative to the bulk solution) appears to be much larger for the laminar-flow experiments than that for the turbulent-flow experiments.

Of the four observations listed above, only the first correctly describes the $CuSO_4$ concentration profiles. Observations 2-4 are artifacts of light-ray deflection (refraction) in the mass-transfer boundary layer. Simple methods of interpretation of interferograms, that neglect light-curvature effects, can lead to large errors(40,41) in derived current densities, concentration changes and boundary layer thicknesses. Quantitative reduction of experimental interferograms to concentration profiles requires extensive computations to account for light-ray curvature effects. Correction procedures of varying degrees of complexity have been developed(26-30, 40-48). In general, larger interfacial refractive-index gradients result in greater light-ray deflection, which in turn requires more complex computational procedures. The present study employed a complex iterative procedure(42), which was shown to be accurate for the steep refractive-index (concentration) gradients expected.

Previous studies of the mass-transfer boundary layer formed by constant-current electrodeposition under laminar channel flow conditions have been reported elsewhere(31). Local steady-state concentration profiles were found to be consistent with well-established heat and mass transfer correlations(38,2,9) and the appropriate solution to the convective-diffusion equation(31), provided that the experimental interferograms were interpreted by the above-mentioned procedure(42) to properly account for light-ray deflection.

Quantitative interpretation of interferograms measured under turbulent flow conditions proved to be very difficult. The interference fringes and the associated derived current densities showed rapid and random fluctuations. Current densities (interfacial concentration gradients) varied between 10% and 100% of the expected values over time intervals of ca. 0.03 sec, as revealed by analysis of high-speed (up to 64 frames/sec) motion-pictures of the interferograms. Concentration differences (between bulk and interface) showed similar fluctuations, while boundary layer thicknesses showed somewhat smaller fluctuations. This observation is an indication that the smoothly-varying, one-dimensional concentration profiles employed in the computational procedure(42) to interpret the interferograms cannot account for the (expected) random perturbations of local concentrations within the mass-transfer boundary layer, caused by turbulent eddy motion. This result could be expected, because the interferometric measurements produce a two-dimensional representation of a three-dimensional concentration field. Local refractive-index information is averaged along the optical path of the test beam, but the stirring action of the turbulent fluid motion can lead to substantial and random variations along the

same optical path, an effect not easily accounted for in the computational procedure to interpret interferograms.

In Fig. 5 the measured Nernst boundary layer thicknesses* in the obstacle-free channel are compared with those predicted by the Chilton-Colburn analogy(49):

$$Sh_{avg} = \frac{d_e}{\delta_N} = \frac{f}{2} Re\ Sc^{1/3} \tag{1}$$

where f is the Fanning friction factor(50), and the other terms are defined in the List of Symbols. The error bars reflect the uncertainty due to the above-mentioned fluctuations in the experimental interferograms. The measured Nernst boundary layer thicknesses show fair agreement with those predicted by the Chilton-Colburn analogy, with the greatest deviations occurring near the leading edge of the cathode, as expected, because the mass-transfer boundary layer is not fully developed in that region. Note that the Nernst boundary-layer thickness at Re = 10,000 is only about 0.03 mm, whereas the precise location of the electrode/electrolyte interface can only be determined (on the interferogram) with an accuracy of ±0.005 mm. It is therefore beyond the practical resolution limit of double-beam interferometry to measure boundary layer thicknesses for Reynolds numbers much larger than 10,000.

Figures 6-9 display interferograms of the concentration field in the immediate vicinity of the four flow obstacles attached to the cathode

*The Nernst boundary layer thickness is defined by the ordinate location where the extrapolated interfacial concentration gradient intersects with the extrapolated bulk concentration.

surface. The following conclusions can be made by inspecting Figs. 6-9:

1. Significant secondary flows are induced by the three larger obstacles at Re = 1500, and all four obstacles have a relatively small effect on the mass-transfer boundary layer at Re = 500.

2. The smaller semi-circular cylinder has little effect at either Re = 500 or Re = 1500.

Consideration of the above observations in light of the sizes of the flow obstacles relative to those of the local mass-transfer boundary layer thicknesses (see Fig. 2) leads one to the following generalization: the secondary flow induced by small flow obstacles significantly thins the local mass-transfer boundary layer only when the characteristic dimension (i.e. the distance that the obstacle protrudes from the electrode surface into the electrolyte) of the obstacle is comparable to, or exceeds the local mass-transfer boundary layer thickness.

Figures 10 and 11 illustrate interferograms of the mass-transfer boundary layers just upstream of, and up to 12.5 cm downstream from, the triangular parallelepiped obstacle attached to the cathode surface. It is seen that the secondary flow induced by the triangular parallelepiped effectively thins the local mass-transfer boundary layer for more than 2.5 cm (33 times the obstacle height) downstream of the obstacle for Re = 1500, and only for about one centimeter downstream from the obstacle at Re = 500.

Conversion of the experimental interferograms of the mass-transfer boundary layers in the presence of flow obstacles at Re = 500 and Re =

1500 was performed exactly as described above for Re = 5,000 and Re = 10,000. Difficulties similar to those encountered for interpretation of interferograms under turbulent flow conditions were experienced when interferograms of the wake regions just downstream of the flow obstacles were analyzed. In Figs. 12 and 13 the Nernst boundary layer thicknesses measured at Re = 500 and Re = 1500 are compared with those predicted by the well-known Norris-Streid correlation(38,2,9)

$$Sh(z) = 1.23 \left(Re\ Sc \frac{d_e}{z}\right)^{1/3} \tag{2}$$

for heat and mass transfer under laminar flow conditions. The measured Nernst boundary layer thicknesses show the expected agreement(31) with the Norris-Streid correlation at locations remote from the vicinity of the flow obstacles. Significant thinning of the local mass-transfer boundary layer is observed only at Re = 1500 for the flow obstacles attached to the cathode surface, which is consistent with the previous qualitative observations of the interferograms. The large cylinder sandwiched midway between the cathode and anode shows the expected reduction of local mass-transfer boundary layer thickness caused by restriction of the flow channel cross sectional area.

It is instructive to compare the effective reduction in local mass-transfer boundary layer thickness caused by placing a flow obstacle on the electrode surface with that obtained by increasing the electrolyte flow rate. For example, Figs. 8, 11 and 13 show that the otherwise laminar mass-transfer boundary layer at Re = 1500 is substantially thinned for at least 2.5 cm downstream from the triangular parallelepiped flow obstacle. The Nernst boundary layer thickness is reduced from about

0.25 mm just upstream from the obstacle to about 0.08 mm 1.5 cm downstream from the obstacle. The electrolyte flow velocity required to produce a Nernst thickness of 0.08 mm can be computed from Eq.(1) to correspond to Re = 2790. The pressure drop (directly related to pumping power and cost) required to maintain a given average flow velocity is given by:

$$\frac{dP}{dz} = 2\ \rho\ v_{avg}^2\ \frac{f}{d_e} \tag{3}$$

Since the friction factor f varies only slightly(50) from $1500 \leq Re \leq 2790$, and the flow velocity v is proportional to the Reynolds Number Re, the ratio of the pressure drop for the two flow velocities considered is approximately

$$\frac{(dP/dz)_{Re=2790}}{(dP/dz)_{Re=1500}} = \left|\frac{2790}{1500}\right|^2 = 3.5.$$

Therefore, reduction of the Nernst thickness from 0.25 mm to 0.08 mm by increasing the electrolyte flow rate requires a 3.5-fold increase in pressure drop.

The corresponding increase in pressure drop caused by attachment of triangular parallelepiped flow obstacles to the electrode surface can be computed from the correlation presented by Leitz et al (3):

$$f = \frac{a}{Re} + 0.175\ n_p\ d_e \frac{1 - \beta^2}{\beta^2} \tag{4},$$

where a is a specific channel dimension parameter, n_p is the number of

promoters per centimeter along the length of the channel, and β is the ratio of the open area perpendicular to the flow at the obstacle to the cross-sectional area of the channel without the obstacle. For the triangular obstacle and the given flow-channel dimensions (Fig. 1), the parameters are $a=16.6$ and $\beta=0.97$. If triangular-parallelepiped flow obstacles were spaced two centimeters apart along the length of the cathode ($n_p = 0.5\ cm^{-1}$), the friction factor f computed from Eq.(4) would increase by a factor of only 1.7 over that for a smooth electrode. Therefore, insertion of triangular-parallelepiped flow obstacles in place of increased flow velocity results in a 70% decrease in pressure drop for the same mass-transfer rate.

The electrolyte pumping costs associated with various means to enhance mass-transport rates at the electrode surface are directly related to the power dissipation, which is the pressure gradient multiplied by the average electrolyte velocity. The power dissipation therefore varies in direct proportion to the friction factor and as the cube of the average electrolyte velocity. Reduction of the Nernst thickness from 0.25 mm to 0.08 mm by increasing the electrolyte flow rate therefore requires a 6.4-fold increase in power dissipation, which may be compared to a 1.7-fold increase in power dissipation caused by insertion of triangular-parallelepiped flow obstacles.

CONCLUSIONS

Double-beam interferometry has been shown to provide qualitative and quantitative information about mass-transfer processes under turbulent flow conditions. Derived mass-transfer boundary layer thicknesses under turbulent flow conditions show the expected agreement with well-established heat transfer correlations.

It is shown that the insertion of certain flow obstacles in an otherwise laminar flow stream can result in increased mass-transfer rates. The increased pressure drop and associated pumping power caused by the presence of the flow obstacle is shown to be substantially less than that required to produce the same increase in mass-transfer rates by an increase in flow velocity.

ACKNOWLEDGEMENT

This work was supported by the Director, Office of Energy Research, Office of Basic Energy Sciences, Materials Sciences Division of the U.S. Department of Energy under contract no. DE-AC03-76SF00098. We also thank the National Aeronautics and Space Administration for a predoctoral fellowship.

This was Paper 157 presented at the Pittsburgh, Pennsylvania meeting of the Society, October 15-20, 1978.

LIST OF SYMBOLS

a	specific channel dimension parameter, see ref. (3)
C	$CuSO_4$ concentration (mol/liter)
d	glass sidewall thickness (cm)
d_e	hydraulic diameter of flow channel (cm)
f	Fanning friction factor (see Ref. 50)
h	electrode separation (cm)
i_{avg}	average current density (mA/cm^2)
L	electrode length (cm)
n_p	obstacle spacing frequency (cm^{-1})
Re	Reynolds number
Sc	Schmidt number
Sh(z)	local Sherwood number
Sh_{avg}	average Sherwood number
v_{avg}	average flow velocity (cm/sec)
w	electrode width (cm)
z	coordinate parallel to electrolyte flow, measured from electrode leading edge (cm)
β	flow channel cross-sectional area contraction coefficient
δ_N	Nernst boundary layer thickness (cm)
λ	light wavelength (cm)
ν	kinematic viscosity (cm^2/sec)
ρ	density (gm/cm^3)

REFERENCES

1. W.H. Safranek and C.H. Layer, Trans. Inst. Metal Finish. 53, 121 (1975).

2. R.E. Acosta, "Transport Processes in High Rate Electrolysis," (Ph.D. Thesis), LBL-2242 (1974), accepted for publication, A.I.Ch.E.J. (1984).

3. F.B. Leitz and L. Marincic, J. Applied Electrochemistry 7, 473 (1977).

4. E. Schalch and N. Ibl, Electrochim. Acta 20, 435 (1975).

5. S. Mohanta and T.Z. Fahidy, Can. J. Chem. Eng. 50, 248 (1972).

6. W.R. Wolfe, H. Chessin, E. Yeager and F. Hovorka, J. Electrochem. Soc. 101, 590 (1954).

7. R.H. Muller, D.J.Roha and C.W. Tobias, Proc. Symp. on Transport Processes in Electrochemical Systems, R. Yeo, T. Katan and D. Chin, eds., Electrochem. Soc. Proc. Vol. 82-10, pp. 1-5 (1982); see also S. Eisner, Plating 58, 995 (1971).

8. J.R. Selman and C.W. Tobias, J. Electroanal. Chem. 65, 67 (1975).

9. J.R. Selman and C.W. Tobias, Adv. Chem. Eng. 10, 211 (1978).

10. J.S. Watson and D.G. Thomas, A.I.Ch.E. J. 13, 676 (1967).

11. G. Belfort and G.A. Guter, Desalination 10, 221 (1972).

12. Y. Winograd, A. Solan and M. Torren, Desalination 13, 171 (1973).

13. F.B. Leitz, L. Marincic, P. Johnson and J. Liston, "Effect of Turbulence Promoters on Local Mass Transfer, 3rd Report," Ionics Technical Report, Waltham, Massachusetts (1974).

14. M.S. Isaacson and A.A. Sonin, Ind. Eng. Chem. Proc. Des. Dev. 15, 313 (1976).

15. A. Storck and F. Coeuret, Electrochim. Acta 22, 1155 (1977).

16. A. Storck and D. Hutin, Can. J. Chem. Eng. 58, 92 (1980).

17. D.H. Kim, I.H. Kim and H.N. Chang, Int. J. Heat Mass Transfer 26, 1007 (1983).

18. W.W. Focke, Electrochim. Acta 28, 1137 (1983).

19. R.H. Muller, in "Advances in Electrochemistry and Electrochemical Engineering," Vol. 9, R.H. Muller, Editor, pp. 326-353, Wiley-Interscience, New York (1973).

20. W. Hauf and U. Grigull, in "Advances in Heat Transfer," Vol. 6, J.P. Hartnett and T.F. Irvine, Editors, pp. 133-366, Academic Press, New York (1970).

21. F.R. McLarnon, R.H. Muller, and C.W. Tobias, Electrochim. Acta 21, 101 (1976).

22. R.N. O'Brien, J. Electrochem. Soc. 113, 389 (1966).

23. A. Tvarusko and L.S. Watkins, ibid. 118, 248 (1971).

24. L. Hsueh and J.S. Newman, Electrochim. Acta 16, 479 (1971).

25. N. Ibl, Y. Barrada and G. Trumpler, Helv. Chim. Acta 37, 583 (1954).

26. Y. Awakura and Y. Kondo, J. Electrochem. Soc. 123, 1184 (1976).

27. Y. Awakura, M. Okada and Y. Kondo, ibid. 124, 1050 (1977).

28. Y. Awakura, Y. Takenaka and Y. Kondo, Electrochim. Acta 21, 789 (1976).

29. N. Ibl and R.H. Muller, Z. Elektrochem. 59, 671 (1955).

30. M. Clifton and V. Sanchez, Electrochim. Acta 24, 445 (1979).

31. F.R. McLarnon, R.H. Muller and C.W. Tobias, Ind. Eng. Chem. Fundam. 18, 97 (1979).

32. C.S. Lin, R.W. Moulton and G.L. Putnam, Ind. Eng. Chem. 45, 640 (1953).

33. F.R. McLarnon, R.H. Muller and C.W. Tobias, J. Electrochem. Soc. 129, 2201 (1982).

34. K.J. Hanson, "Interferometric Study of Mass Transfer Enhancement by Turbulence Promoters," (M.S. Thesis), LBL-9038 (1979).

35. F.R. McLarnon, Ph.D. Thesis, LBL-3500, University of California, Berkeley (1975).

36. K.W. Beach, Ph.D. Thesis, UCRL-20324, University of California, Berkeley (1971).

37. K.W. Beach, R.H. Muller and C.W. Tobias, Rev. Sci. Instrum. 40, 1248 (1969).

38. R.H. Norris and D.D. Streid, Trans. ASME 62, 525 (1940).

39. F.R. McLarnon, R.H. Muller and C.W. Tobias, Appl. Optics 14, 2468 (1975).

40. K.W. Beach, R.H. Muller and C.W. Tobias, J. Opt. Soc. Am. 63, 559 (1973).

41. F.R. McLarnon, R.H. Muller and C.W. Tobias, J. Electrochem. Soc. 122, 59 (1975).

42. F.R. McLarnon, R.H. Muller and C.W. Tobias, J. Opt. Soc. Am. 65, 1011 (1975).

43. U. Grigull, Int. J. Heat Mass Transfer 6, 669 (1963).

44. W.L. Howes and D.R. Buchele, J. Opt. Soc. Am. 56, 1517 (1966).

45. E.E. Anderson, W.H. Stevenson and R. Viskanta, Appl. Optics 14, 185 (1975).

46. A.M. Hunter and P.W. Schreiber, ibid. 14, 634 (1975).

47. C.M. Vest, ibid. 14, 1601 (1975).

48. C. Forgacs, J. Leibovitz, R.N. O'Brien and K.S. Spiegler, Electrochim. Acta 20, 555 (1975).

49. D.W. Hubbard and E.N. Lightfoot, Ind. Eng. Chem. Fund. 5, 370 (1966).

50. W.L. McCabe and J.C. Smith, Unit Operations of Chemical Engineering (McGraw-Hill, NY, 1967), p. 102.

FIGURE CAPTIONS

Figure 1. Semiscale drawing of the flow channel: channel width w = 10.0 mm, channel height h = 25.4 mm, and electrode length L = 100.0 cm.

Figure 2. Placement and sizes of obstacles in the flow channel.

Ordinate: distance from cathode surface (mm).

Abscissa: distance from cathode leading edge (cm).

The 0.28-mm semi-circular cylinder is attached to the cathode surface at z = 22 cm, the 0.76-mm semi-circular cylinder at 32 cm, the 0.76-mm triangular parallelepiped at 47 cm, the 0.76-mm rectangular parallelepiped at 62 cm, and the 12.7-mm diameter large circular cylinder is wedged between the two glass sidewalls at z = 82 cm.

- - - - : Mass transfer boundary edge (Eq.2), calculated as twice the Nernst boundary layer thickness(33).

Figure 3. Schematic diagram of interferometer and electrochemical cell: ——, light path; ---, off-axis rays demonstrating point-to-point relationship between plane of focus and film plane; A, copper anode; C, copper cathode; E, 0.1M $CuSO_4$ electrolyte; F, film plane; G, glass sidewalls; L, lens (The test lens, focal length = 87 mm, is 115 mm from the center of the cell. The focal length of the reference lens is 81 mm); M, mirror; S, light source (HeNe laser); U, beam uniter; d, thickness of glass wall (12.7 mm); h, electrode separation (2.54 mm); w, electrode width (10.0 mm).

Figure 4. Experimental interferograms showing the effect of electrolyte flow velocity on steady-state mass-transfer boundary layer thickness.

Ordinate: distance from the cathode surface (mm).

Figure 5. Turbulent boundary-layer thicknesses.

Ordinate: Nernst boundary layer thickness δ_N (mm).

Abscissa: Distance z from cathode leading edge (cm).

————: Thickness computed from Eq.(1).

- - - - : Represents uncertainty of computed values due to a 10% uncertainty in diffusion coefficient data.

O : Derived from experimental interferograms, Re = 5000, i_{avg} = 15.0 mA/cm^2.

△ : Re = 5,000, i_{avg} = 25.0 mA/cm^2.

□ : Re = 10,000, i_{avg} = 25.0 mA/cm^2.

Figure 6. Experimental interferograms of the 0.28-mm semi-circular cylinder. The electrolyte flow is from left to right.

left: $i_{avg} = 0.$

center: Re = 500, $i_{avg} = 2.0$ mA/cm^2.

right: Re = 1500, $i_{avg} = 2.5$ mA/cm^2.

Figure 7. Experimental interferograms of the 0.76-mm semi-circular cylinder. Designations as in Fig. 6.

Figure 8. Experimental interferograms of the 0.76-mm triangular parallelepiped. Designations as in Fig. 6.

Figure 9. Experimental interferograms of the 0.76-mm rectangular parallelepiped. Designations as in Fig. 6.

Figure 10. Experimental interferograms of the region near the 0.76-mm triangular parallelepiped. Re = 500, $i_{avg} = 2.0$ mA/cm^2. The electrolyte flow is from left to right.

a: z = 46.5 cm

b: z = 47.0 cm

c: z = 47.5 cm

d: z = 49.5 cm

e: z = 59.5 cm

Figure 11. Experimental interferograms of the region near the 0.76-mm triangular parallelepiped. Re = 1500, $i_{avg} = 2.5$ mA/cm^2. Designations as in Fig. 10.

Figure 12. Nernst boundary-layer thicknesses at Re = 500.

Ordinate: Nernst-boundary layer thickness (mm).

Abscissa: reduced distance z/L from cathode leading edge.

● : derived from experimental interferograms.

———: Norris and Streid correlation(38).

- - - - : boundary layer-thicknesses near obstacles.

a: z = 22 cm, location of smaller semi-circular cylinder.

b: z = 32 cm, larger semi-circular cylinder.

c: z = 47 cm, triangular parallelepiped.

d: z = 62 cm, rectangular parallelepiped.

e: z = 82 cm, large circular cylinder.

Figure 13. Nernst boundary layer thicknesses at Re = 1500. Designations as in Fig. 12.

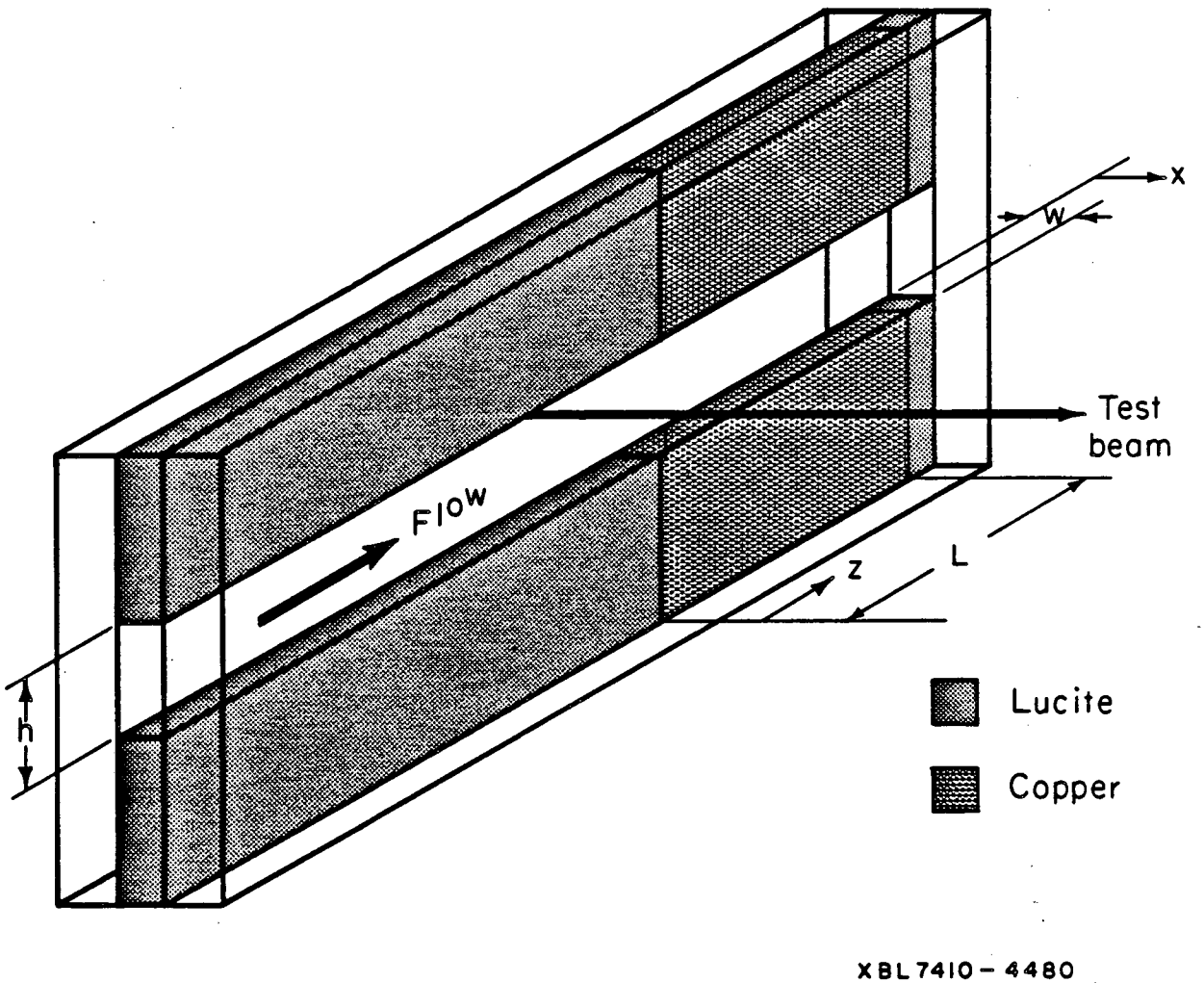

Fig. 1

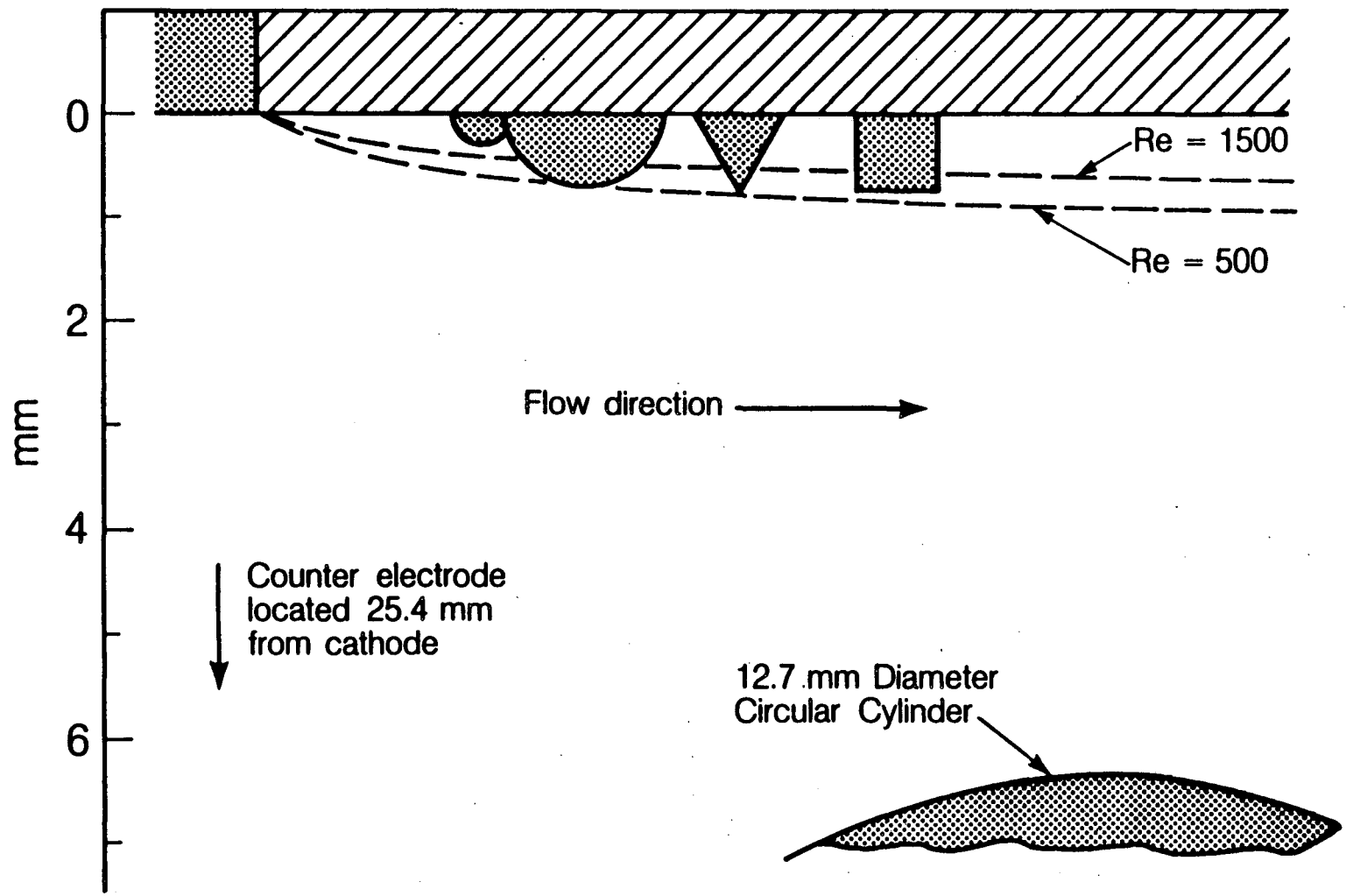

XBL 8410-8796

Fig. 2

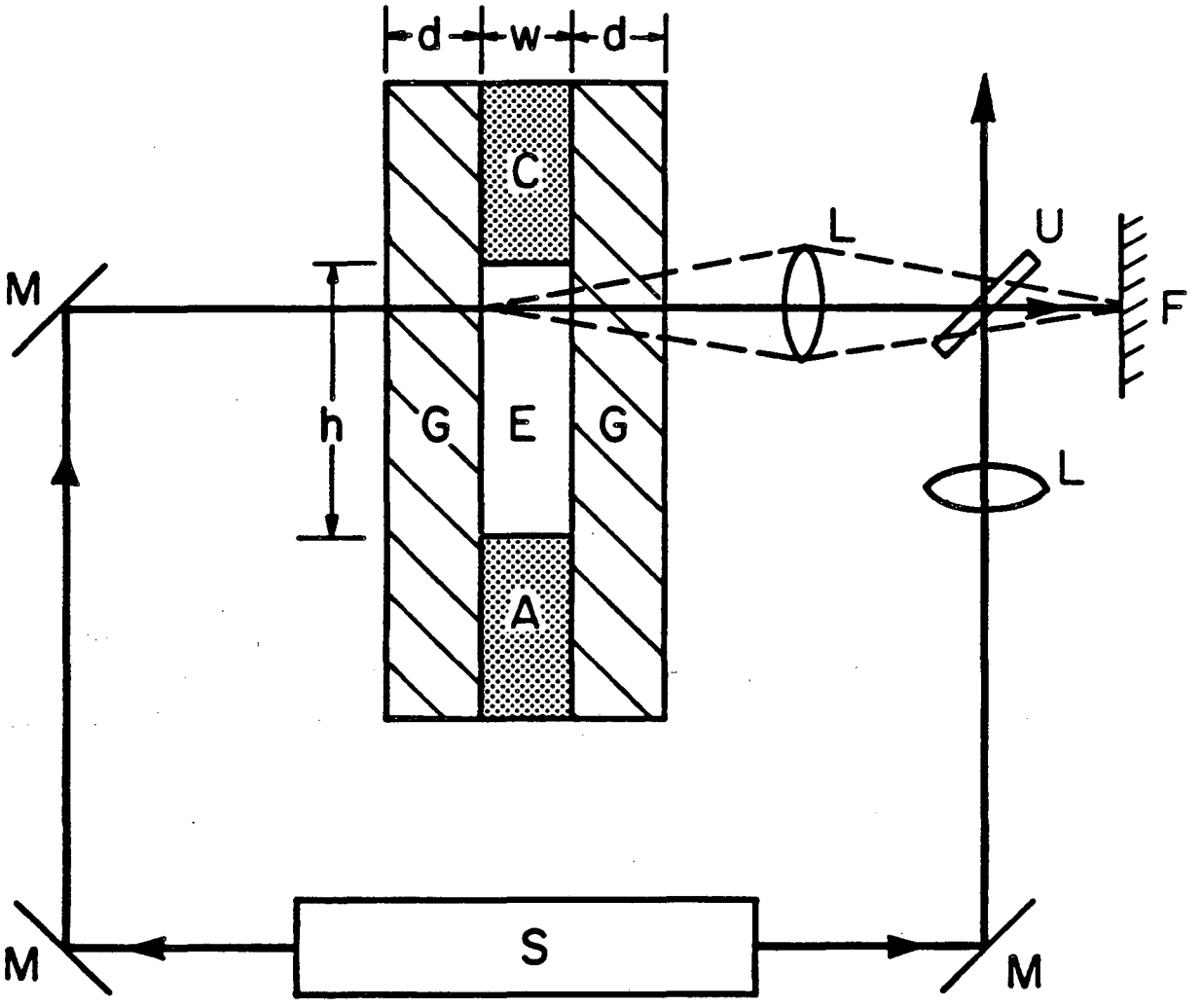

XBL749-4165

Fig. 3.

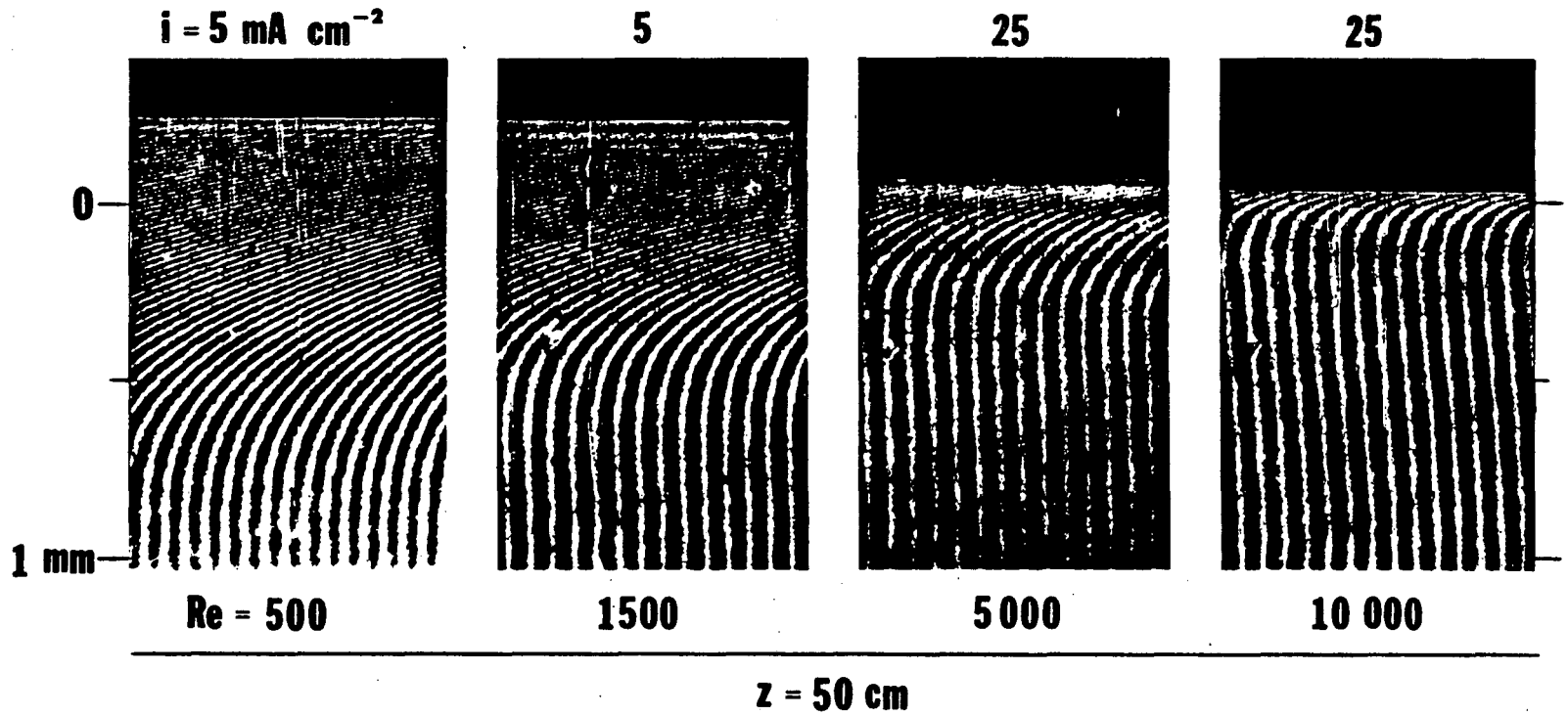

XBB 748-5798

Fig. 4

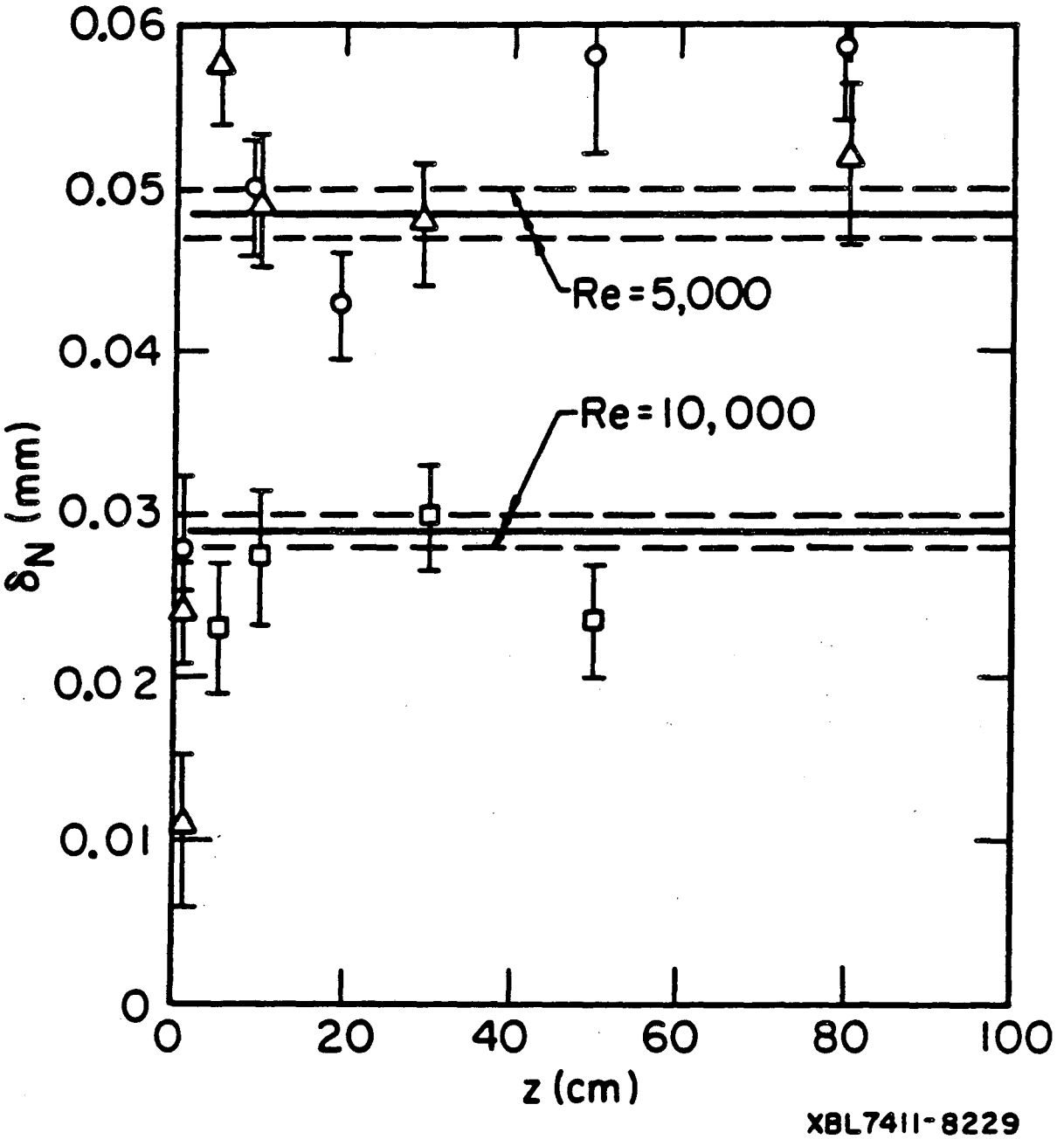
0.06
0.05
0.04
0.03
0.02
0.01
0
δ_N (mm)
Re=5,000
Re=10,000
0
20
40
60
80
100
z (cm)
XBL7411-8229

Fig. 5

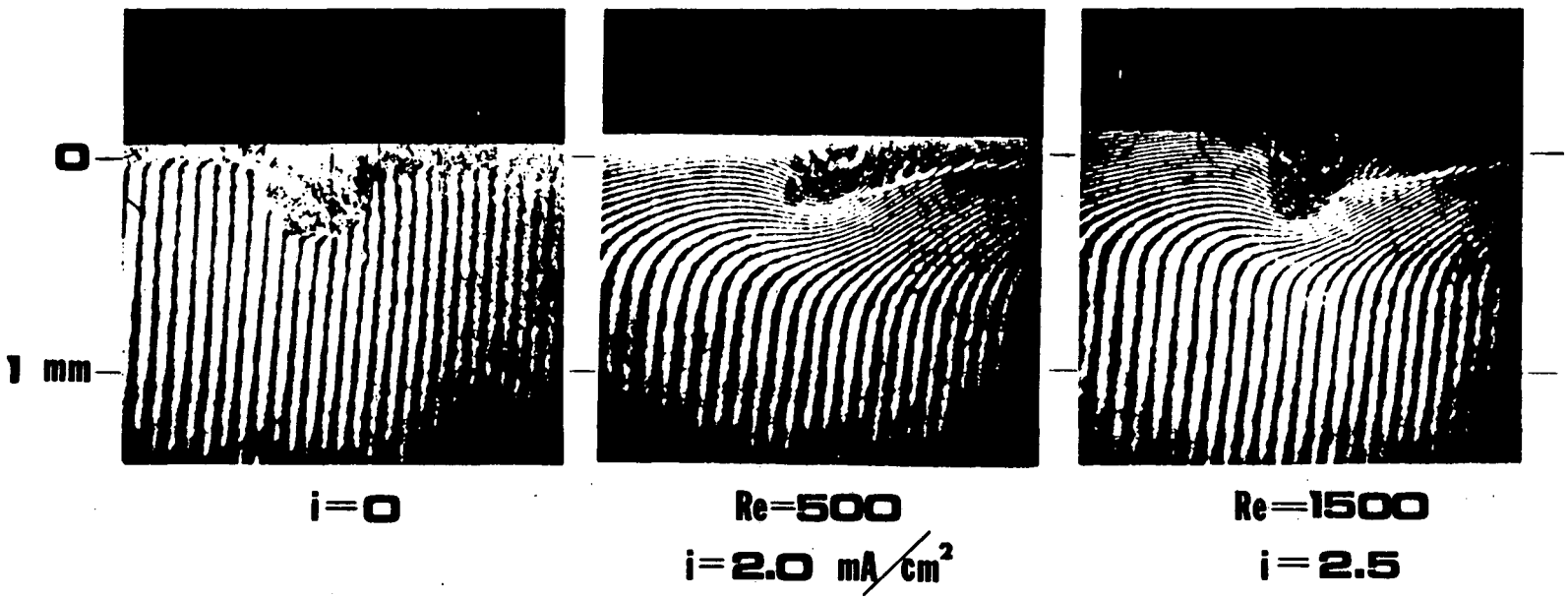

XBB 740-8122

Fig. 6

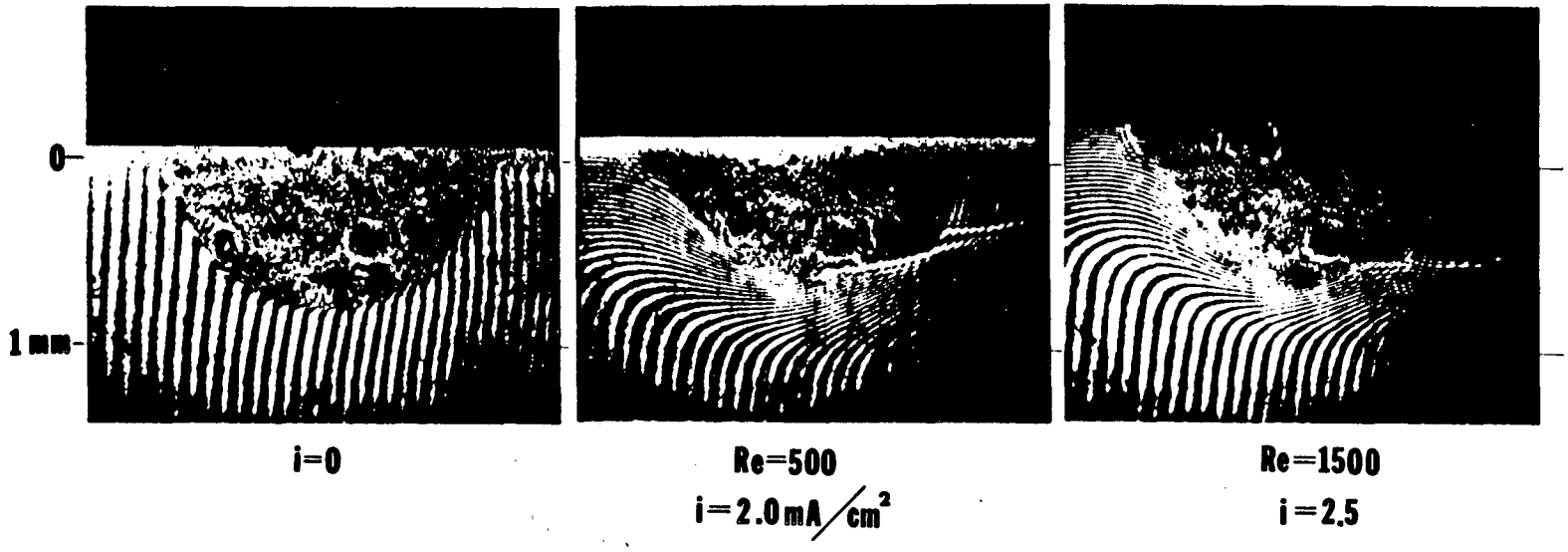

XBB 740-8121

Fig. 7

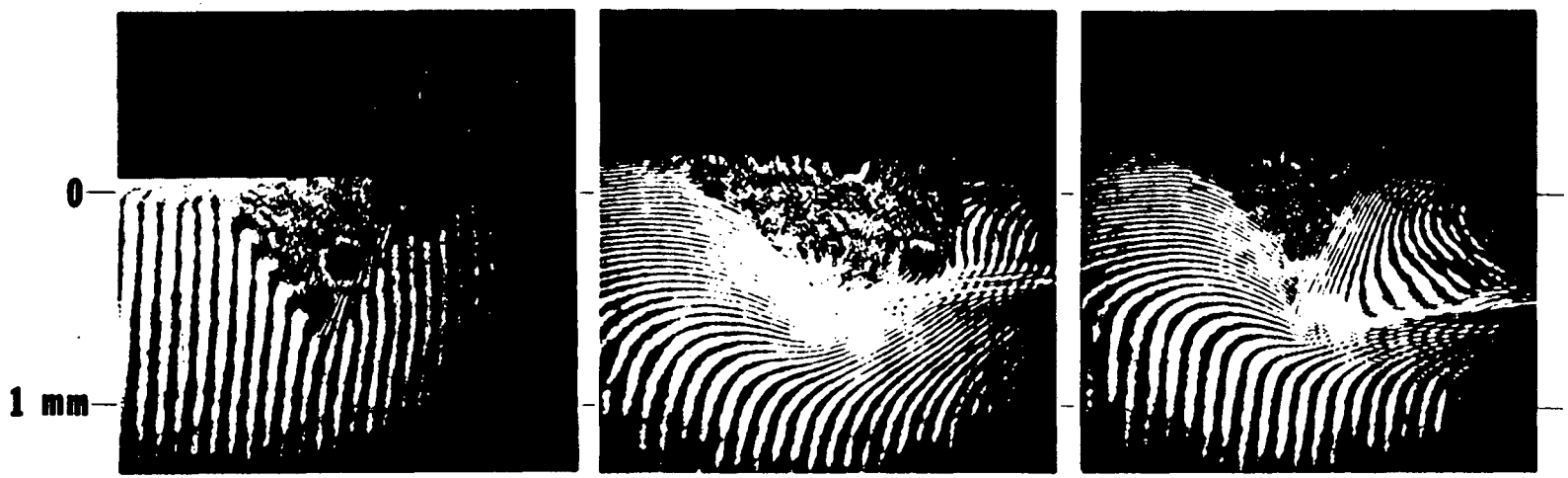

i = 0

Re=500
i = 2.0 mA/cm²

Re=1500
i=2.5

XBB 740-8123

Fig. 8

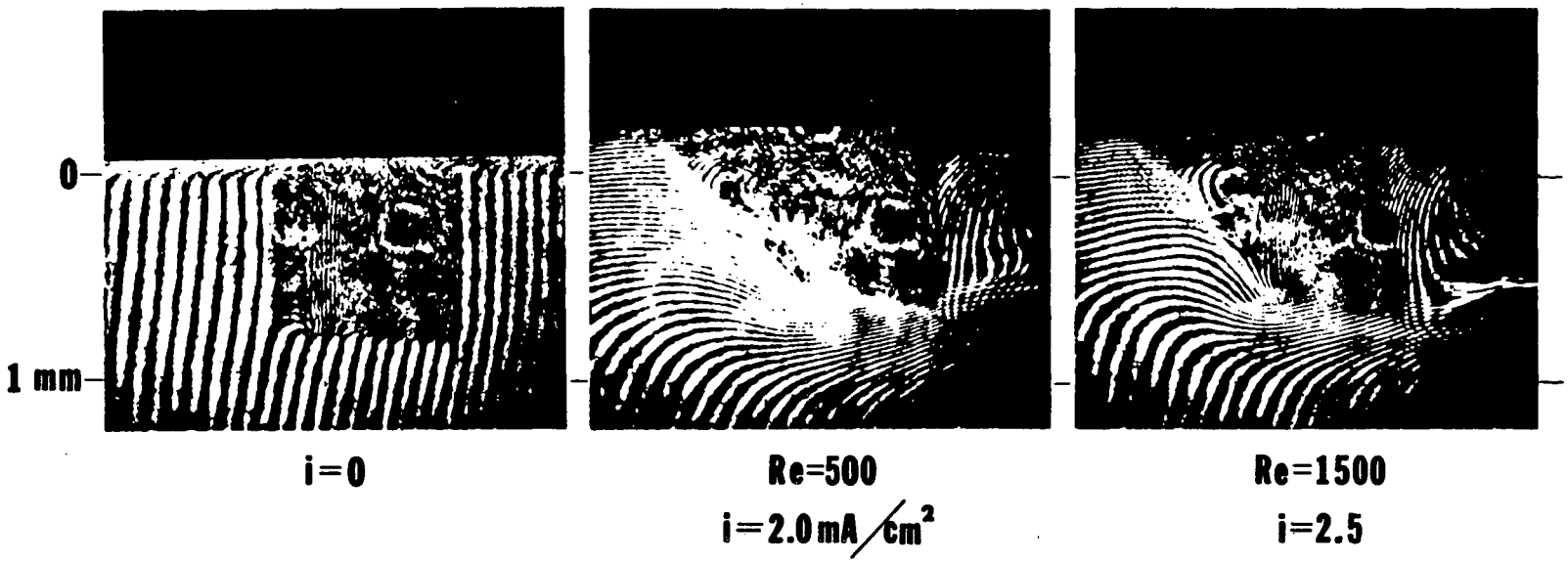

XBB 740-8124

Fig. 9

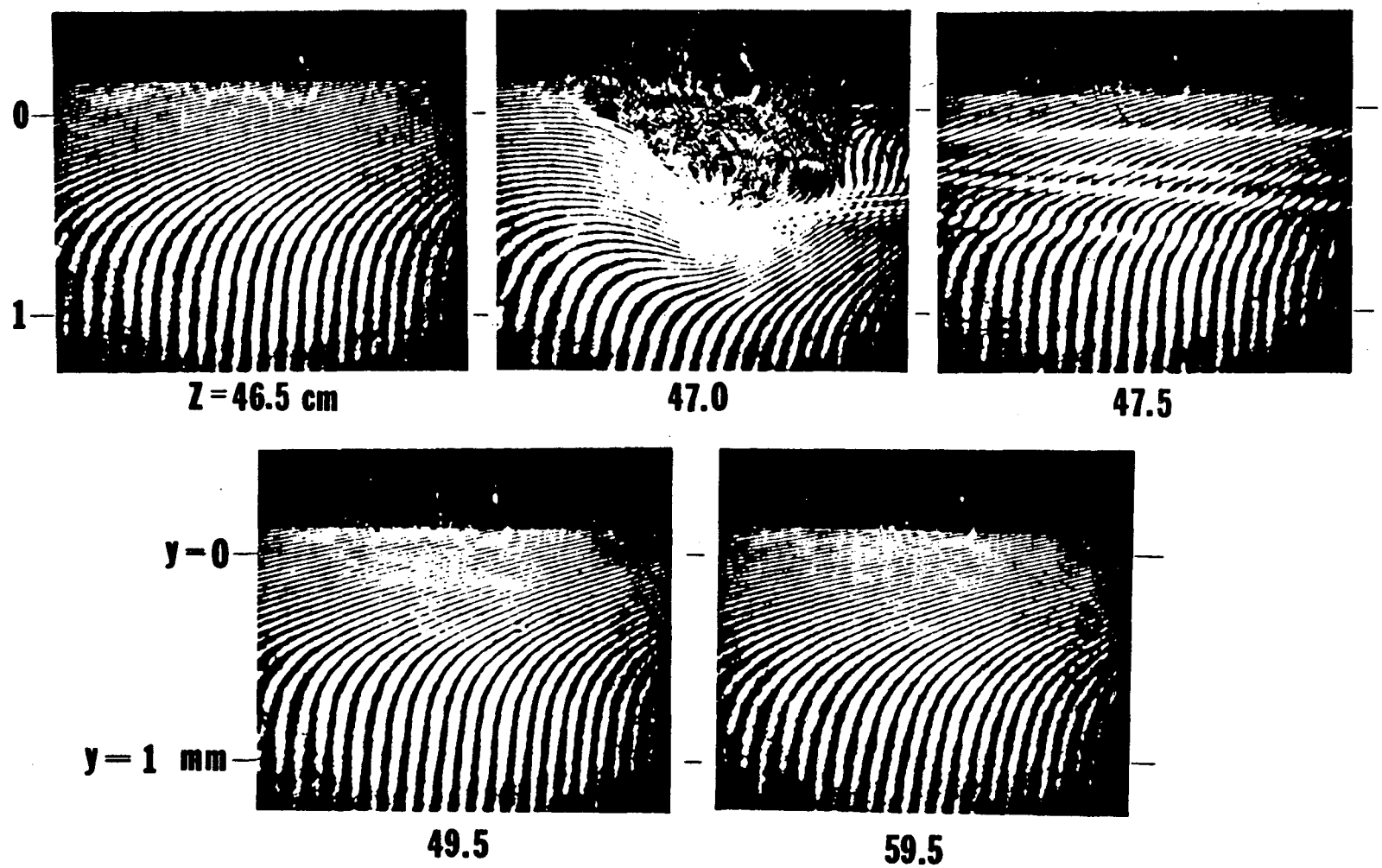

Re=500 i=2.0 mA/cm^2

XBB 740-8125

Fig. 10

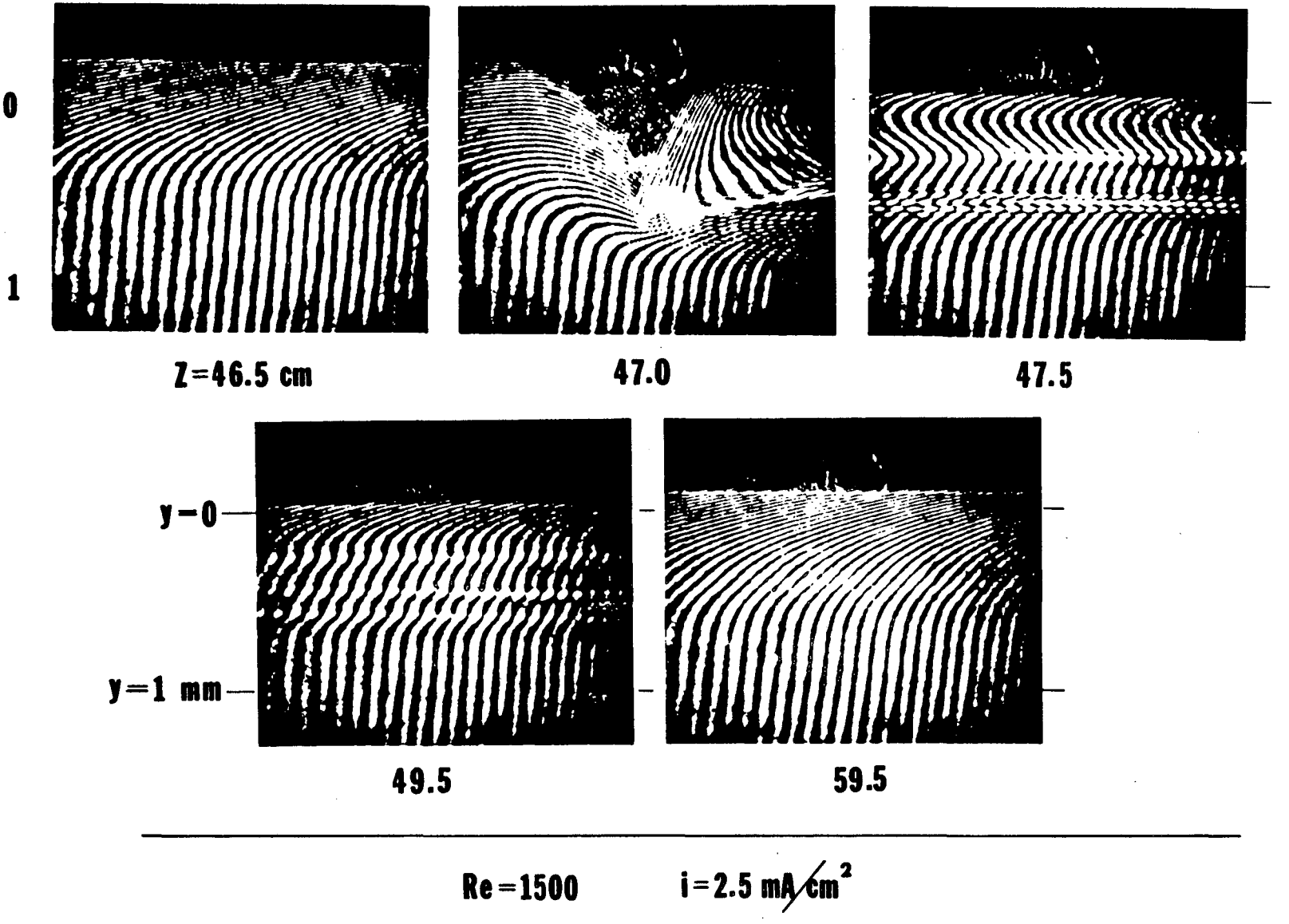

XBB 740-8126-B

Fig. 11

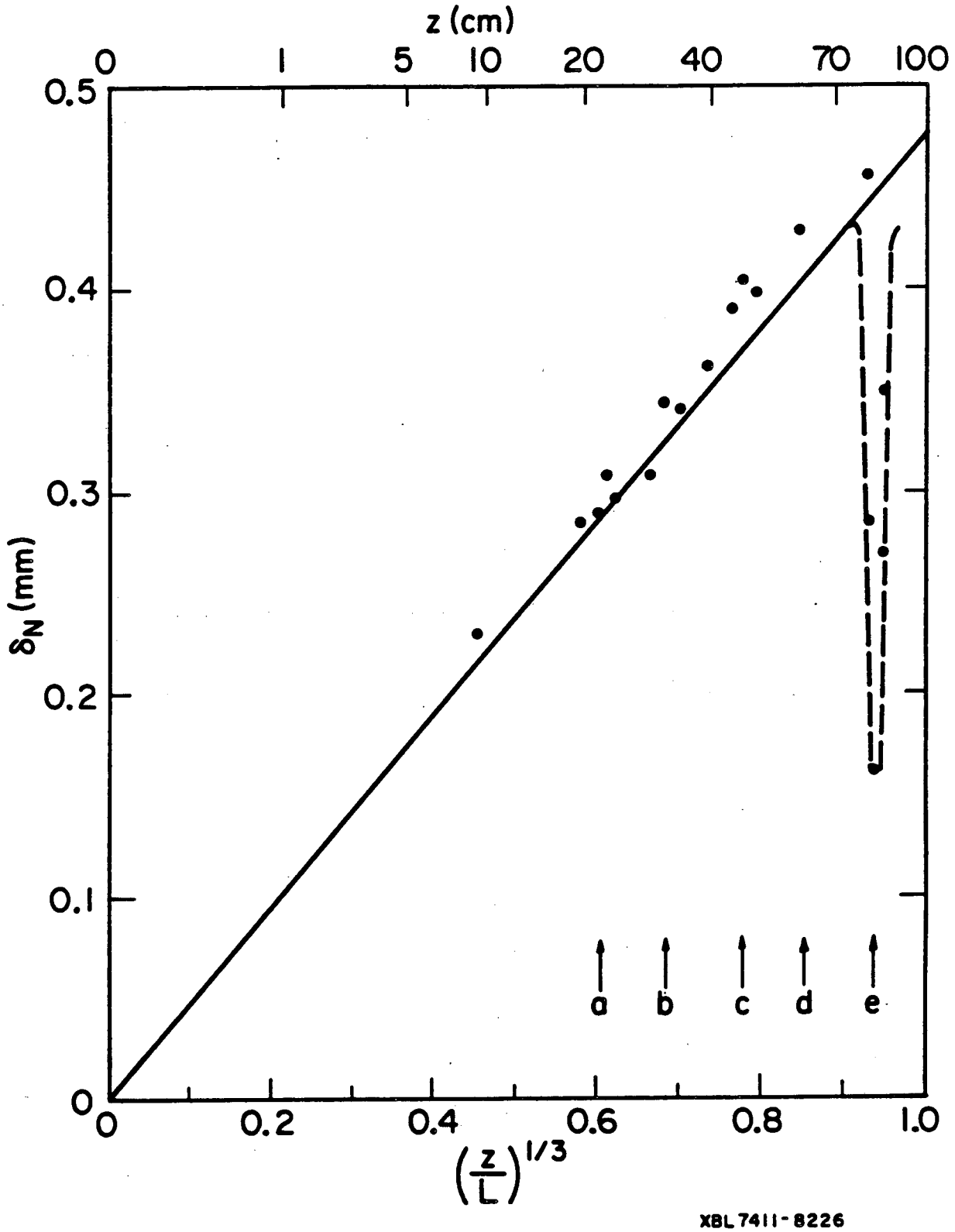
z (cm)
0
1
5
10
20
40
70
100
0.5
0.4
0.3
0.2
0.1
0
δ_N (mm)
a
b
c
d
e
0
0.2
0.4
0.6
0.8
1.0
$\left(\frac{z}{L}\right)^{1/3}$
XBL 7411-8226

Fig. 12

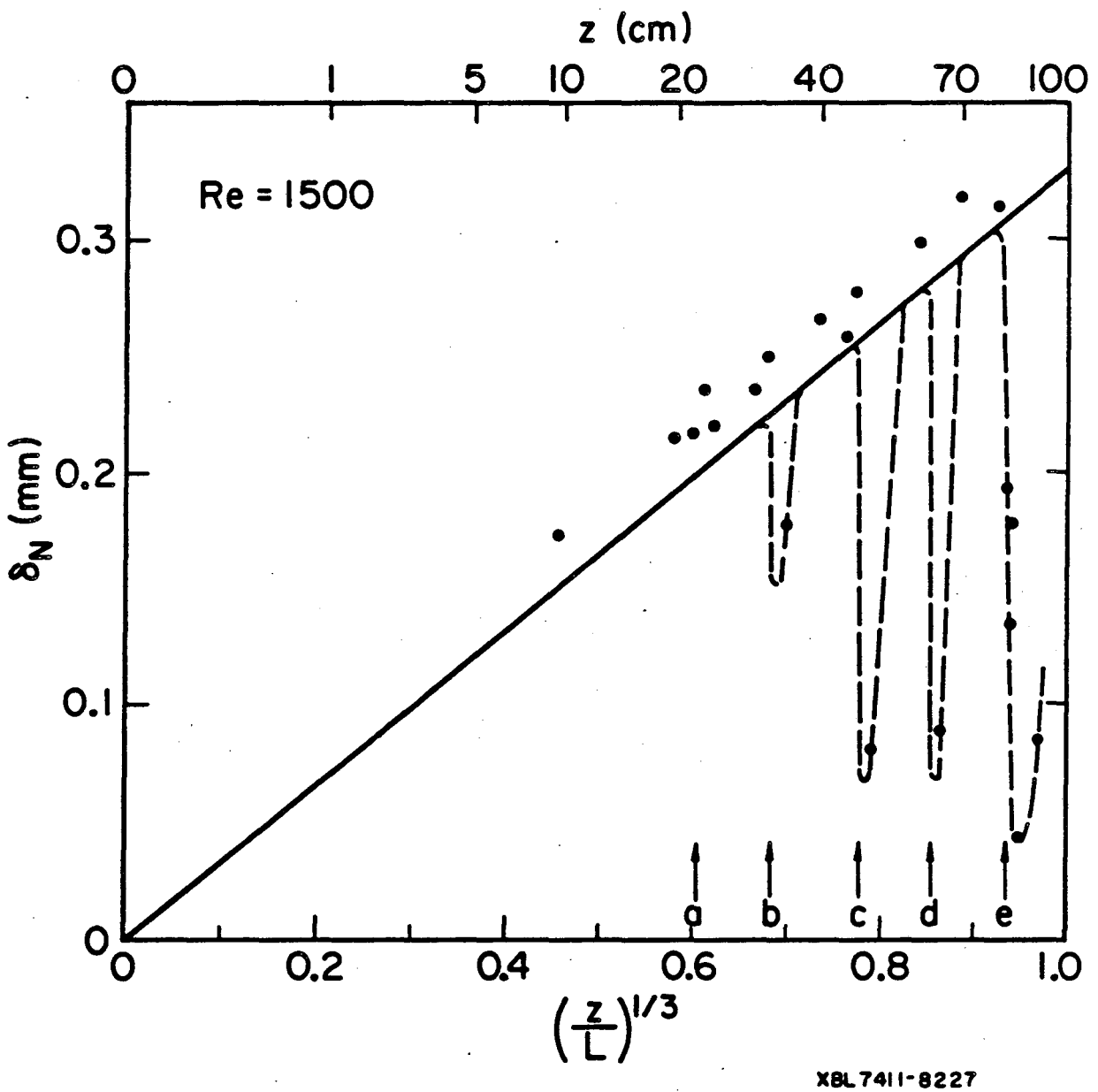
z (cm)
0
1
5
10
20
40
70
100
Re = 1500
0.3
0.2
0.1
0
δ_N (mm)
a
b
c
d
e
0
0.2
0.4
0.6
0.8
1.0
$\left(\frac{z}{L}\right)^{1/3}$
XBL7411-8227

Fig. 13

This report was done with support from the Department of Energy. Any conclusions or opinions expressed in this report represent solely those of the author(s) and not necessarily those of The Regents of the University of California, the Lawrence Berkeley Laboratory or the Department of Energy.

Reference to a company or product name does not imply approval or recommendation of the product by the University of California or the U.S. Department of Energy to the exclusion of others that may be suitable.

TECHNICAL INFORMATION DEPARTMENT
LAWRENCE BERKELEY LABORATORY
UNIVERSITY OF CALIFORNIA
BERKELEY, CALIFORNIA 94720